



Analysis of a Severe Dust Storm Event over China: Application of the WRF-Dust Model

Hai Bian¹, Xuexi Tie^{2,3}, Junji Cao^{3*}, Zhuming Ying⁴, Suqin Han¹, Yong Xue⁵

¹ Tianjin Meteorological Bureau, Tianjin, China

² National Center for Atmospheric Research, Boulder, CO, USA

³ SKLLQG, Institute of Earth Environment Science, Chinese Academy of Science, Xian, China

⁴ Department of Earth and Atmospheric Science, York University, Toronto, Canada

⁵ Institute of Remote Sensing Applications, Chinese Academy of Science, Beijing, China

ABSTRACT

A severe dust storm (SDS) event occurred during March-20 to March-22, 2010 in China. A regional dynamical model coupled with a dust model (WRF-Dust) is used for analyzing this SDS event. The distribution of API (air pollution index) values in China and satellite (moderate-resolution imaging spectroradiometer—MODIS) AOD (aerosol optical depth) data are used to trace the dust storm and to compare with the model result. Several model sensitive studies are performed to analyze the roles of physical processes (such as dust source, transport, and deposition) in controlling the SDS event. The result suggests that the Gobi Desert is a major dust source of the SDS event. By contrast, the Taklamakan Desert plays minor roles for affecting the high dust concentrations in eastern/southern China during the SDS event. This study also suggests that a large amount of dust particles was deposited at the surface during the transport pathway between the Gobi Desert and eastern/southern China, and the high surface concentrations of dust particles can be considered as a new dust source region, which produced dust air pollution when surface winds were strong. In this study, we define this process as a propagate dust source (PDS). The calculation shows that the calculated dust concentrations were considerably lower than the measured values in the downwind regions of deserts when the PDS process was not included in the model. By including the PDS process, the calculated dust pollution in eastern and southern China is considerably improved. The further detailed analysis shows that the PDS played important roles in controlling the long-range transport of dust particles during the SDS event. This study suggests that this regional dust model (WRF-Dust) is a useful tool to analyze the important processes of dust storms that are often occurred in China.

Keywords: Severe dust storm; Eastern China; WRF-Dust model.

INTRODUCTION

Massive dust storms were often occurred in deserts of northwestern China and Mongolia during springtime. The dust storms were transported to downwind regions, causing high particle concentrations and extremely low visibility in these regions (Lee *et al.*, 2009). These “Asian dust storms” (ADSs) are originated mainly from two large deserts, such as the Taklamakan Desert in XinJiang Province of China and the Gobi Desert located in Inner Mongolia of China and southern Mongolia (Singer, 1988; Gomes and Gillete, 1993; Rost, 2001; Shao and Dong, 2006; Cao *et al.*, 2008; Tie and Cao, 2009). The occurrence of the ADSs is strongly related to weather and soil conditions in the desert

regions. During wintertime, the soil is frozen or covered by snow, and is not easily released into air to form dust storms. However, during springtime, the soil temperature increases and the soil moisture is low in these desert regions. Under such conditions, soil dust is ready to be released into atmosphere to form a dust storm. Weather condition is also crucial for the formation of dust storms. When wind speed is greater than 10 m/s, it has a strong energy to blow soil particles from surface to the atmosphere. In order to drive dust particles to high altitudes, an unstable atmosphere which is generally associated with upward motion is also required. During springtime, mid-latitude cyclone systems (normally associated with strong winds and upward motions) often pass through in western China. These weather systems are generally associated with strong winds and upward motions, which lift dust particles from surface to about 1 to 3 km altitudes and lead to the particles to be transported to the downwind of the desert regions (Lee *et al.*, 2009; Gu *et al.*, 2010; Stone *et al.* 2011). The Asian

* Corresponding author.

E-mail address: cao@loess.llqg.ac.cn

dust storms are usually carried by northwesterly or westerly winds over northern and eastern China. However, in some cases, these dust storms can also be transported to southern/eastern part of China where the population density is very high, leading to significant impacts on human's life in the populated regions over China (Zhao *et al.*, 2009; Zhang *et al.*, 2010; Zhao *et al.*, 2011).

The massive ADSs have important impacts on environment, human life, and ecosystem. For example, the ADSs produce severe visibility reductions with lowest visibility of less than 200 meters. The ADSs can significantly affect the human's health, causing respiratory symptoms and eye trouble (Takayama and Takashima, 1986; Kim *et al.*, 2002). As pointed out by Mikami *et al.* (2009), the ADSs also have important effects on weather and climate change. The dust particles in the atmosphere affect the radiative forcing of the atmosphere via scattering and absorbing shortwave and longwave radiation through both direct and indirect ways (Tomey, 1991; Sokolik *et al.*, 2001). Once the mineral dust particles deposited in the ocean they act as a source of nutrients which cause changes in the primary production of phytoplankton (Duce *et al.*, 1980). This process is one of the major factors in the carbon dioxide cycle on a global scale and has important implication for global climate change (Dayan *et al.*, 1991; Duce *et al.*, 1991).

During March-19 to March-22, 2010, a severe dust storm (SDS) occurred in northwestern China and Mongolia, and propagated to eastern/southern China, affecting human's life in a large area. In addition, the dust storm extended in a long period of time (about 4 days). During this period, the aerosol particle concentrations reached to considerably high values, and caused extremely low ranges of visibility. Thus, this SDS event should be intensively studied, and the result of the study could provide scientific information for better understanding the origins and transport pathways of dust storms in this region.

This study focuses on the analysis of the SDS event. A regional dynamical/dust model (WRF-dust) is applied to study the origin and the pathway of the SDS event. The model calculation is compared with the spatial and temporal variations of PM₁₀ concentrations (derived from air pollution index (API)). Detailed transport and deposition processes of the SDS event are investigated by analyzing model result and meteorological conditions. Several sensitive studies are conducted to study the impact of various sources (or different deserts) on the dust distribution and the pathway of the dust storm. A brief description of WRF-Chem model with dust processes is given in section 2. In section 3, the model results and comparison with the measurements are presented. In section 4, the detailed model analysis is conducted.

WRF-DUST MODEL

A regional dynamical model (version 3 of Weather Research and Forecasting model – WRF-v3) is used in this study. An important objective of this study is to simulate the distribution of dust particle and to investigate the

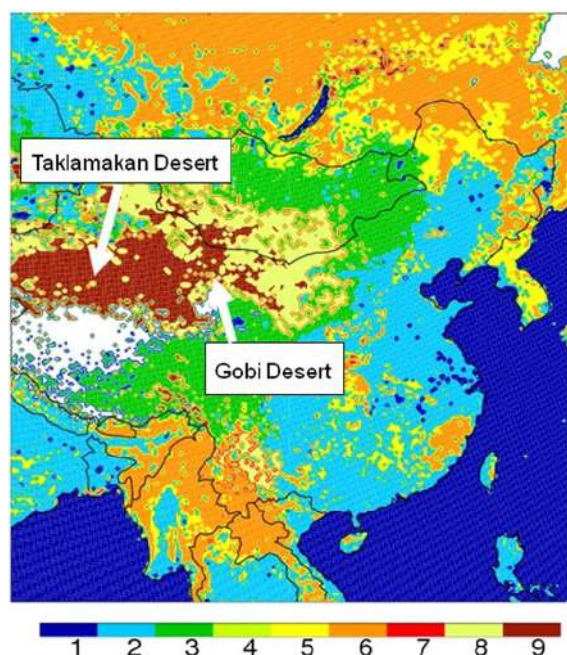
processes which play important roles in controlling the severe dust storm (such as dust source, transport, and deposition). The model includes 2 major parts, i.e., a dynamical model (WRF) and a dust model. The Weather Research and Forecasting (WRF) model is a mesoscale numerical weather prediction system designed to serve both operational forecasting and atmospheric research needs. The WRF model is a fully compressible and Euler nonhydrostatic model. The Yonsei University (YSU) PBL scheme [Hong *et al.*, 2006] is used for calculating PBL height in this study. The detailed description of WRF model can be found in the WRF web-site <http://www.wrf-model.org/index.php>. In addition to dynamical calculations, a dust model is coupled on-line with the WRF model, and the coupled model is defined as the WRF-Dust model.

The physics of dust, such as dust emissions, transport, dry deposition, and gravitational settling in WRF-Dust are the same as the dust modules developed by the GOCART model (Georgia Tech/Goddard Global Ozone Chemistry Aerosol Radiation and Transport model). Dust emission is dependent on the surface properties (such as soil composition, vegetation, and soil moisture content), and on surface wind velocity (Grini *et al.*, 2005). Soil erosion is the derive force of the suspend particle emissions and erosion threshold is based on the size distribution of the erodible soils and the roughness length of the surface (Marticorena and Bergametti, 1995), which is defined as dust source erodibility. In large desert areas, erodibility is strongly determined by desert properties and large erodibility is often occurred in desert regions (Ginoux *et al.* 2001). The dust erodibility thus is estimated by the surface land conditions (USGS data), and shows in Fig. 1. It shows that there are two major deserts (Taklamakan Dessert and Gobi Desert) in northwestern of China and Mongolia. Taklamakan Desert locates at far west of China and is the largest desert in China. Gobi Dessert locates in middle-west China and south of Mongolia. During winter and spring time, the prevailing winds are generally northwest winds. As a result, the dust storms originated in these deserts often have important effects on the populated areas of China (such as eastern coast of China).

The dust particles have 5 size bins with mean radius of 0.6, 1.2, 2.4, 4.5, and 8.0 μm , respectively (see details in Table 1). The dust emission in each dust particles size bins is size-resolved, which is calculated by taking into account the soil particle fraction, erosion factor, surface wind velocity, and the threshold velocity of wind erosion. The flux F_p at particle size bin p is determined by the following expression:

$$F_p = \begin{cases} C\alpha_p E_r V_s^2 (V_s - V_t) & V_s > V_t \\ 0 & \text{otherwise} \end{cases} \quad (1)$$

Where C is a dimensional factor ($C = 0.8 \text{ugs}^2 \text{m}^{-5}$), α_p is the soil particle fraction at size bin p , E_r is the probability soil erosion factor, v_s is surface wind velocity at 10 m and v_t is the threshold velocity of wind erosion. The threshold velocity is determined as a function of the particle size and density, and the soil moisture (Ginoux *et al.*, 2001).



1 = Water bodies; 2 = Cropland + Pasture; 3 = Grassland; 4 = Shrubland; 5 = Savanna; 6 = Forest; 7 = Wetland; 8 = Mixed Tundra; 9 = Desert

Fig. 1. Surface landscape map in China. The dark brown color indicates the location of the largest deserts (Taklamakan and Gobi Deserts) in China.

Table 1. Classification of API index and the corresponding concentrations of PM_{10} .

API (i)	C(i)
50	50
100	150
200	350
300	420
400	500
500	600

After dust particles are emitted under favorable meteorological conditions (dry and windy days), the particles are transported, are dry deposited and are gravitational settled at surface. The detailed descriptions of these processes are given by Ginoux *et al.* (2001).

A DUST EVENT DURING MARCH 20–22, 2010

Measured Dust Storm

During March/20–22, 2010, a SDS occurred in a large area of China, and has serious impacts on human's life in the region. In order to analyze this nationwide event, the measured API (air pollution index) is used to analyze the severe dust event. The API measurement is conducted by environment protection administration of China (EPAC), and the data is published daily (see <http://datacenter.mep.gov.cn/>) for 86 cities in China. The use of API index has its advantages and disadvantages for the study of the SDS event. During the SDS event, the dust particles spread out

in a large area in China. Thus, a nationwide of aerosol data network is required to study this dust event and to trace the dust storm. Because there are no other symmetrical measurement networks to provide such data, the API network provides valuable information to study the distribution of the dust storm. However, the API index is a combination value of several air pollutants (such as SO_2 , NO_2 , CO, O_3 , and PM_{10}), and a conversion from the API value to dust aerosol concentration is required. However, several uncertainties are remained in the conversions. First, the API index is determined by the highest value of the air pollutants (shown in above). The API index value can either be gas-phase pollutants (SO_2 , NO_2 , CO, and O_3) or particle pollutant (PM_{10}). In this study, all API values with gas pollutants are filtered out from the consideration of the dust storm, and only API values with PM_{10} (API_ PM_{10}) are remained. Second, the API_ PM_{10} values also contain some small particles (PM_1 and $PM_{2.5}$). These small particles are partially attributed to the anthropogenic particle emissions in industrial area, especially in eastern China. As a result, the API_ PM_{10} values often overestimate the dust particle concentrations (a positive bias effect). Finally, the API values have a highest cap (500), which limits the dust concentrations to be less than $600 \mu\text{g}/\text{m}^3$ (see Table 2). During the SDS event, however, the dust concentrations are often higher than $600 \mu\text{g}/\text{m}^3$. In this case, a negative bias occurs due to the cap of API values. In order to get the insight of the effects of the “positive and negative biases”, the measurement of PM_{10} and $PM_{2.5}$ concentrations is shown in Fig. 2. The aerosols were measured with R&P1400a (manufactured by American R&P Company) with Tapered Element Oscillating Microbalance (TEOM) technology. The measurement was made in Tianjin ($117^\circ 13'E$, $39^\circ 07'N$), China, located in the eastern coast of China. During the SDS event, the daily averaged PM_{10} concentrations reached to the highest value ($500 \mu\text{g}/\text{m}^3$) on March-20, 2010, and gradually reduced to $100 \mu\text{g}/\text{m}^3$ on March-23, 2010, indicating that the SDS event mainly occurred between March-20 and March-22. The measurement also shows that during the SDS period, the mass of larger particles of $PM_{10-PM_{2.5}}$ (with radius between 2.5 and $10 \mu\text{m}$) were significantly higher than the mass of smaller particles of $PM_{2.5}$ (with radius less than $2.5 \mu\text{m}$). For example, on March-20 the mass was 500 and $90 \mu\text{g}/\text{m}^3$ for PM_{10} and $PM_{2.5}$, respectively. The mass of large particles ($PM_{10-PM_{2.5}}$) was about 82% of total mass (PM_{10}), suggesting that the measured aerosol mass was dominated by large dust particles. This result also give a rough estimate that the “positive bias” is about 20% when the API values are used to estimate dust particles. The highest daily averaged values of was about $500 \mu\text{g}/\text{m}^3$, which is under the limitation of API value. In this case, it seems that the “negative bias” was not a serious problem when the API values are used to estimate dust particles. However, this SDS spreads out in a very large area, and some very high concentrations of dust particles could be larger than the cap value of API index. As a result, the “negative bias” should be an important consideration when the API values are used to estimate dust particles. By

Table 2. Information regarding the gravity deposition to surface for different size dust particles.

Bins	Averaged radius R (μm)	Gravity settling velocity V_d (cm/s)	Time required (Days) to deposit at surface From 1 km altitude
1	0.73	0.0387	29.8
2	1.40	0.1509	7.66
3	2.40	0.4436	2.60
4	4.50	1.5597	0.74
5	8.00	4.9297	0.23

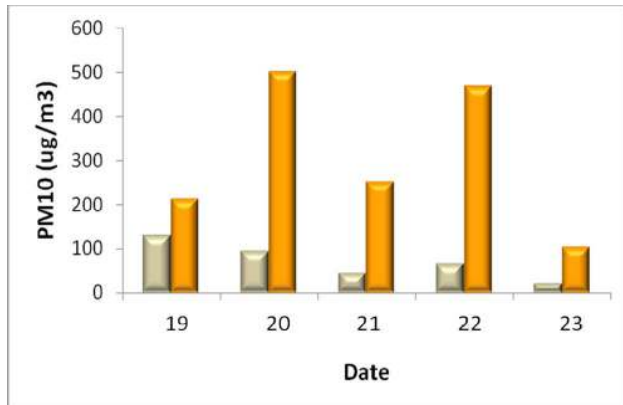


Fig. 2. Measured PM_{10} and $\text{PM}_{2.5}$ concentrations ($\mu\text{g}/\text{m}^3$) in Tianjin (located in central-eastern China during the severe dust storm (SDS) period (March-19 to March-23, 2010). The yellow bars represent for the PM_{10} and the green bars for $\text{PM}_{2.5}$.

considering both the “positive and negative bias” limitations, the distribution of the API values used in this study is mainly applied to trace the pathway of the dust storm, and cannot be used for the precise comparison between calculated and measured dust concentrations.

Fig. 3 shows the distribution of PM_{10} concentrations during the SDS period (March-19 to March-22). The conversion from the API values to PM_{10} concentrations are according to the conversion factors (see Table 1) and the following equations

$$\text{API} = (\text{API}_{i+1} - \text{API}_i) \times (X - C_i) / (C_{i+1} - C_i) + \text{API}_i \quad (2)$$

$$X = (C_{i+1} - C_i) \times (\text{API} - \text{API}_i) / (\text{API}_{i+1} - \text{API}_i) + C_i \quad (3)$$

Where API and X represent the measured API values and the corresponding PM_{10} concentrations. API_i (API_{i+1}) and C_i (C_{i+1}) represent the API values and the corresponding PM_{10} concentrations at i^{th} ($i^{\text{th}+1}$) levels (shown in Table 1).

The result shows that on March-19, there was an indication that high dust concentrations were not been transported to eastern China and were limited in the source regions (desrt areas). However, due to the lack of the measured API values in the source regions (see Fig. 1 and the circled areas in Fig. 3), there was only one measurement site nearby the source region showing high PM_{10} concentration ($300 \mu\text{g}/\text{m}^3$). On March-20, there was a clearly evident that the high dust concentrations had been

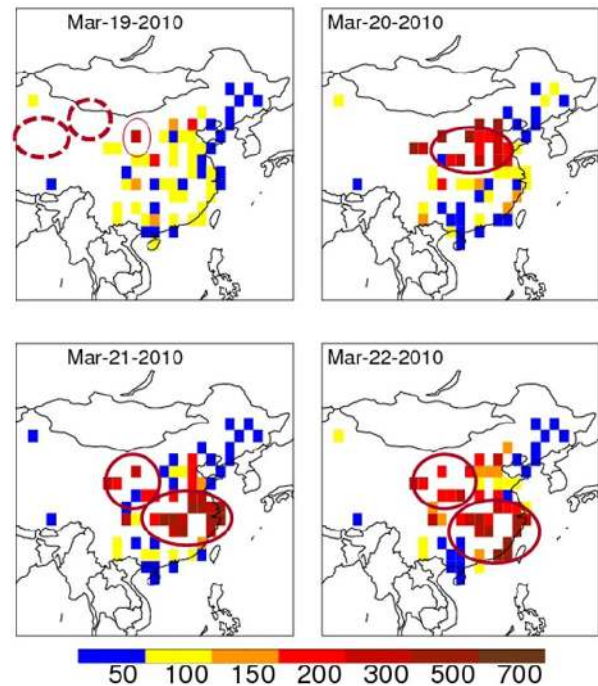


Fig. 3. Measured PM_{10} concentrations ($\mu\text{g}/\text{m}^3$) which are converted from the API values during the SDS period (March-19 to March-22, 2010). The solid line circles indicate the dust storm locations. The dash line circles indicates the large desert areas (where data is missing).

transported to central-eastern China. In central-eastern China, the daily averaged PM_{10} concentrations reached to about $500\text{--}700 \mu\text{g}/\text{m}^3$ (shown by a red circle). On March-21, there were two high PM_{10} concentration regions. One occurred nearby the source region and another happened in southeastern China. On March-22, there was an indication that the dust storm spread out in a large region in eastern China, and large amount dust particles had been transported down to deep southeastern region (such as Guangzhou and Hongkong areas).

Satellite measurements (such as MODIS) were often used to study heavy aerosol pollution in eastern China (e.g., Zhang *et al.*, 2006). However, due to the limitation of the data retrieval (such as cloud effect), it is difficult to obtain a clearly regional aerosol distribution during the SDS events. As a result, only the distribution of aerosol optical depth (AOD) from MODIS measurement during March-21, 2010 are shown in this study (see Fig. 4). It shows the distribution of AOD was very similar to the API result,

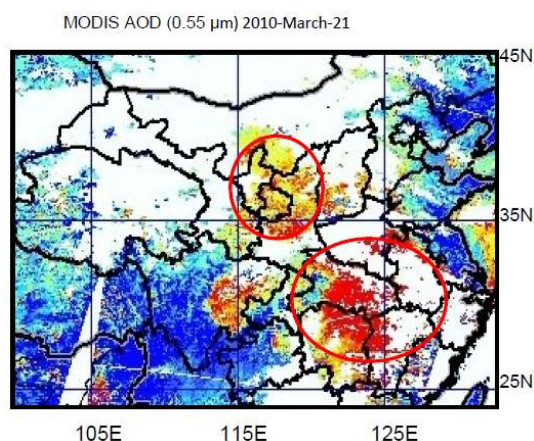


Fig. 4. Measured AOD (aerosol optical depth) at $0.55 \mu\text{m}$ from satellite (MODIS) during the SDS period on March-21, 2010. The solid line circles indicate the dust storm locations.

showing that there were two high dust regions on March-21. The first one occurred in central-north China (close to Gobi Desert) and the second one occurred in southeastern China. The good agreement between the API and AOD values suggests that the distribution of API values is capable to use for studying the SDS event, specially for tracking the dust plums.

The above result suggests that this SDS event had the following particular features, such as: (1) During March-19 to March-22, a large amount of dust particles was generated and was spread out in a large area of eastern China during the SDS event. (2) The dust particles were transported from the source regions to downwind regions between March-20 and March-22. (3) The pathways of the dust storm in the downwind regions were considerably different during different days of the SDS event. On March-20, the downwind transport was westerly, which is often the cases for dust storms in China. By contrast, during March-21 and March-22, the downwind transport was southwesterly, leading to large dust pollution in southern China, which is less happened in China.

Meteorological Conditions during the Dust Storm

In order to understand the transport pathways during the SDS event, the meteorological conditions (weather maps) are shown in Fig. 5. Fig. 5(a) shows that at the afternoon (14 pm) of March-19, there were two low pressure systems (LPS) over China. The first LPS located in and nearby northwestern China, and the second LPS located in central-eastern China. The air between the two LPS was squeezed by the two LPS. As a result, an air pressure ridge with a strong air pressure gradient occurred between the 2 low pressure systems (located in or nearby Gobi Desert). Due to the strong pressure gradient, heavy surface winds (15–20 m/s) were generated in the Gobi Desert area, and a severe dust storm was produced. Fig. 5(a) also shows that the dust storm moved toward southwesterly, producing high dust concentrations in the downwind region (central-eastern China) on March-20. By contrast, another

large desert (Taklamakan Desert) located in the back of first LPS, and the winds were not as strong as in Gobi Desert, and the dust storm generated in Taklamakan Desert is weaker than the one in Gobi Desert. Furthermore, the dust particles in Taklamakan Desert moved toward the southeasterly, and produced important dust pollution in the Tibet Plateau region, but rather than eastern China.

At the afternoon (14 pm) of March-20, the strength of the first LPS significantly decreased, and a high pressure system (HPS) was formed in the Inner-Mongolia region, and the second LPS moved to Yellow Sea. Eastern China was located in between the HPS and the LPS, and strong winds were produced due to the strong pressure gradient in the region, moving the dust storm toward south of central-eastern China.

MODEL ANALYSIS OF THE DUST STORM

Model Calculation of the Dust Storm

The model calculation of the SDS is compared with the measured result during March-19 to March-22, 2010. The comparison between the model calculation and measurement focuses on the following issues; (1) to evaluate model processes, and (2) to analyze the dust storm by using the model calculation. The model calculation (see Fig. 6) shows that on March-19, the calculated dust concentrations in the dust region (Taklamakan and Gobi Deserts) were extremely high ($500\text{--}700 \mu\text{g}/\text{m}^3$), indicating that the model is capable to produce the SDS in the source region. The calculated dust distribution also indicates that the dust storm was limited in the source region, and did not have significant effects on eastern China, which is consistent to the measured result. On March-20, the calculated dust storm was transported westerly from the source region to central-eastern China, which is also consistent to the measurement. However, compared to the measured high dust concentrations ($500\text{--}700 \mu\text{g}/\text{m}^3$), the calculated dust concentrations ($100\text{--}150 \mu\text{g}/\text{m}^3$) were considerably lower than the measure values in central-eastern China. This large underestimation suggests that during the transport processes of the dust storm, some important processes were missing. On March-21 and March-22, the calculated dust storm was mostly constrained in the source region, with an indication that small amount of dust particles were transported southwesterly to southeastern China. However, compared with the measured values, the calculated dust concentrations were much lower than the measured values in southeastern China, suggesting that the dust model needs to be improved in order to simulate the high dust concentrations in the downwind region.

The Propagation of Dust Source

One of the important processes, which is not included in the standard dust model, is that the dust particles are relatively large in size with radius of 0.7 to $8.0 \mu\text{m}$ (see Table 2 for the particle bin 1 to bin 5). The large particles can be easily deposited to surface along transport pathways. Table 2 shows that the gravity settling velocity for the different size of dust particles. It shows that the gravity

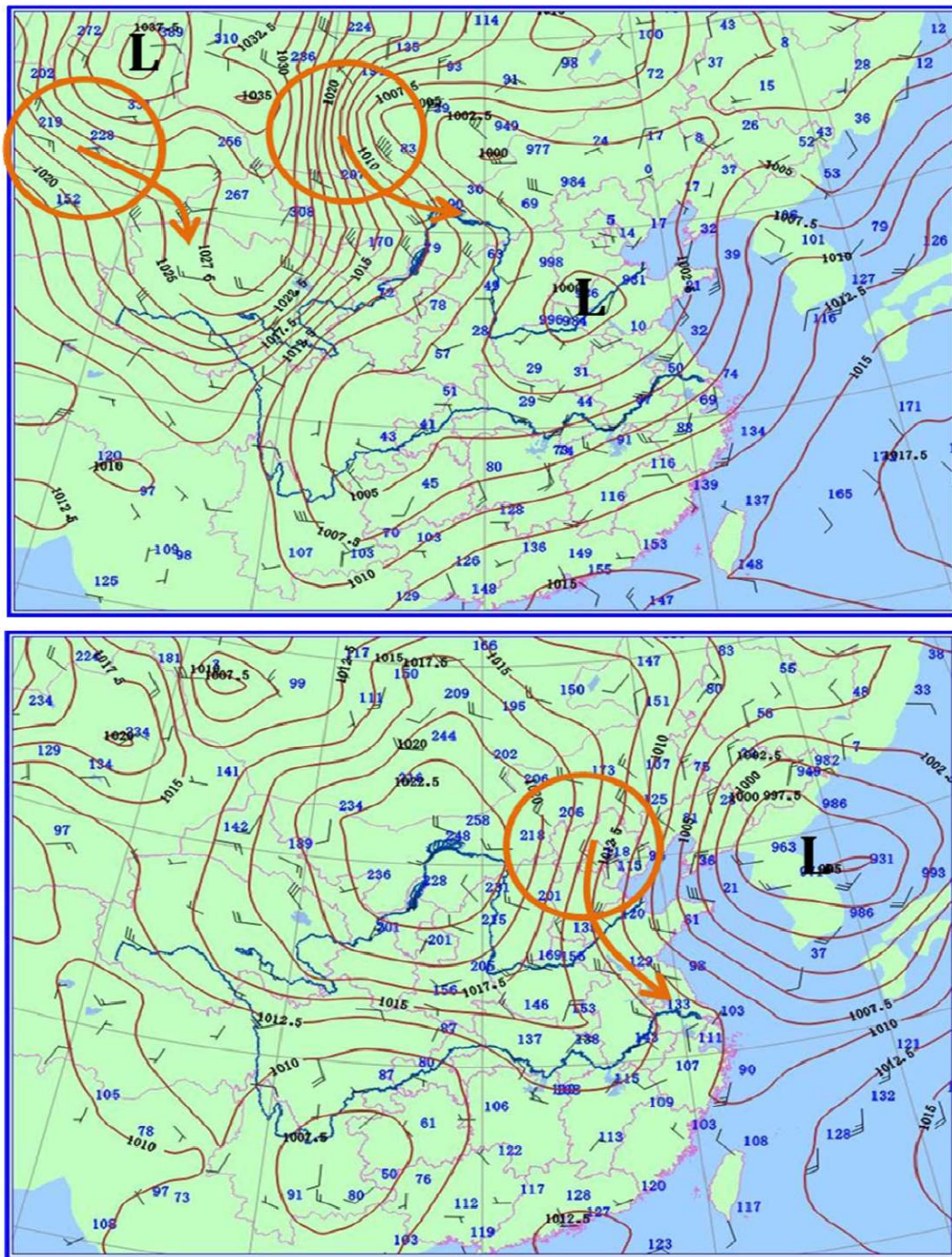


Fig. 5. Weather map at 14pm on Mar-19,2010 (upper panel) and Mar-20, 2010 (lower panel). The brown circles indicate the dust source regions, including the propagated source region.

settling velocities are 0.039, 0.151, 0.444, 1.560, and 4.930 cm/s for the 5 bin dust particles, respectively. If we assume that the dust particles in the dust storm were vertically distributed at altitudes between 0.5 to 1.5 km, the dust particles take 15–45 (bin 1), 3.8–11.5 (bin 2), 1.3–3.9 (bin 3), 0.37–1.1 (bin 4), and 0.11–0.34 (bin 5) days to deposit to surface when they were transported from the source region to eastern China. With wind speed of 5 m/s, the dust particles can be transported to about 43,000 (bin 1), 3,300 (bin 2), 1,100 (bin 3), 320 (bin 4), and 100 km (bin 5) in

the downwind regions. The distance between the dust source region and eastern China is about 2000–3000 km, meaning that the large dust particles (in bin 3, bin 4, and bin 5) were deposited to the surface along the transport pathways. According to the model calculation, the dust mass of large particles (in bin 3, bin 4, and bin 5) was about 60% total mass of dust particles, suggesting that large amounts of dust particles were deposited at surface during the pathway between the source region and eastern China. The areas where there are heavy surface dust

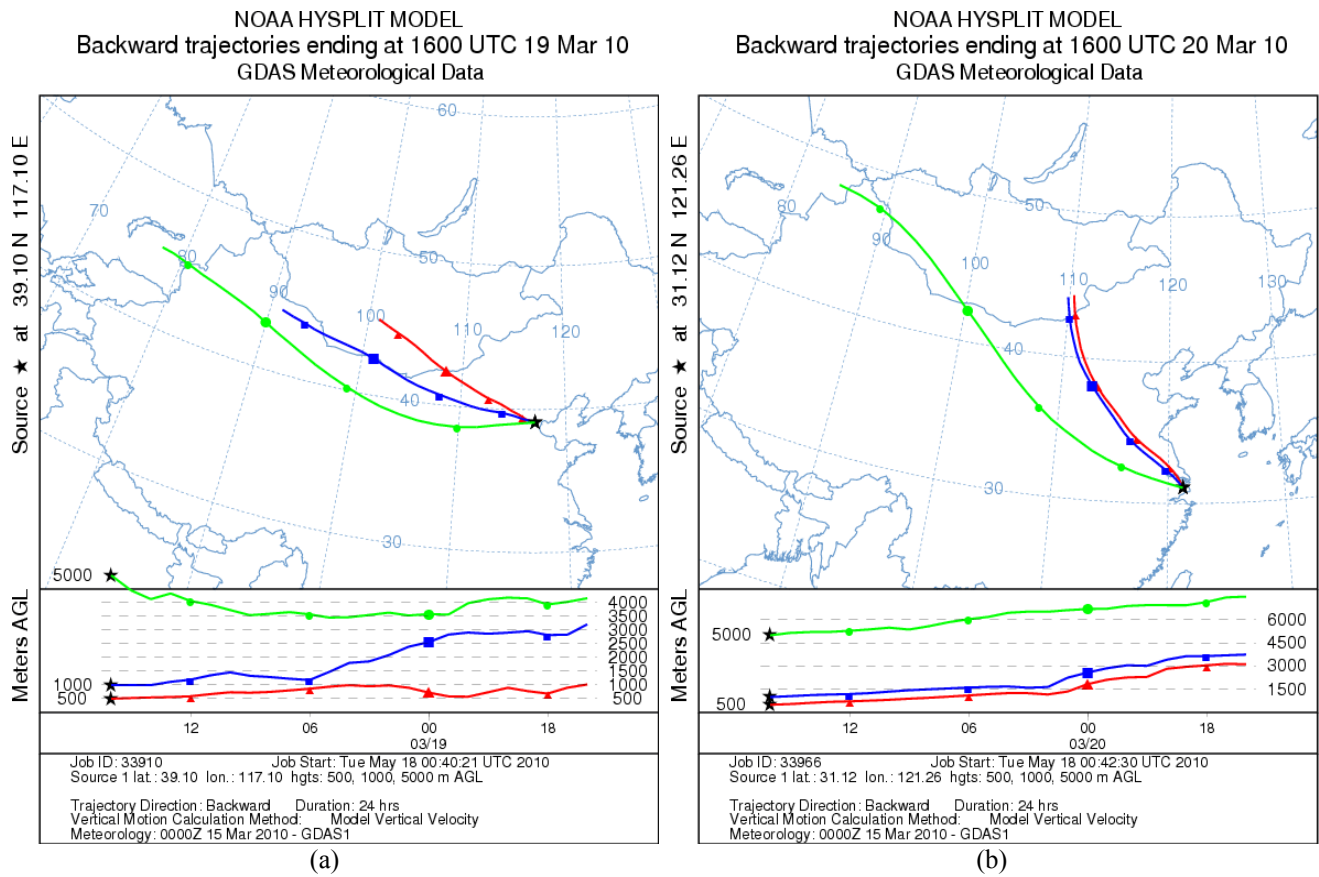


Fig. 6. Backtrajectory from central-eastern China at late of March-19 (Fig. 6(a)) and from south-eastern China at late of March-20 (Fig. 6(b)) at 3 different altitudes (0.5, 1.0, and 5.0 km).

concentrations can be considered as a new dust source region, which produce dust air pollution when surface winds are strong. In this study, we define this process as a propagate dust source (PDS). Furthermore, a back trajectory study is applied to study the PDS. Fig. 6(a) shows the back trajectory from central eastern China (at 117.10°E longitude and 39.80°N latitude) at the late of March-19, It shows that in the lower altitudes (0.5 and 1.0 km), the dust particles were transported from the Gobi Desert region, where the dust storm was originated in this region (see Fig. 6(a)). However, at the late of March-20, when the dust storm started to move to southeastern China, the dust particles were transported from central-eastern China (see Fig. 6(b)) rather than from the originated dust regions (desert areas). This result suggests that the PDS plays important roles when dust particles have been transported for a long distance of downwind region.

Fig. 7 shows the calculated dust storm when the PDS is included in the dust model. The result shows that (see Fig. 7) on March-19, the calculated dust concentrations in the dust source region (Taklamakan and Gobi Deserts) were high (larger than 700 $\mu\text{g}/\text{m}^3$), and the high dust concentrations were limited in the source regions. On March-20, the calculated dust storm was transported westerly from its source region to central-eastern China, and the calculated dust concentrations reached to about 300–500 $\mu\text{g}/\text{m}^3$ in central-eastern China, showing a significant

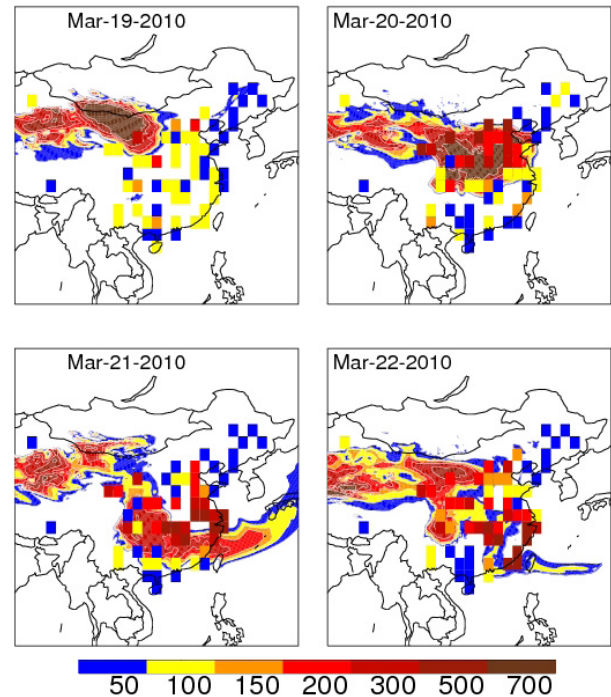


Fig. 7. The measured and calculated dust concentrations ($\mu\text{g}/\text{m}^3$) during the SDS period (March-19 to March-22, 2010). The squares and the contour lines represent the measured and the calculated values, respectively.

improvement compared with the calculation without the PDS. However, there were still some discrepancies between model measured results, indicating some uncertainties of the model. On March-21, the calculated dust storm was transported to southeastern China with dust concentration of 200–300 $\mu\text{g}/\text{m}^3$, which was consistent to the measured values. Although the model calculation for the SDS is significantly improved, there were still some discrepancies between the calculated and measured dust concentrations. For example, on March-22, the calculated dust concentrations were underestimated the measured values in southeastern China.

The Origination of the Dust Storm

In order to better understand the origination of the SDS, several model sensitive studies are conducted. For example, the model calculations by including and excluding Taklamakan Desert as the dust source are performed. The net result of the two calculations gives the calculated dust storm due to only Takalamakan Desert (shown in Fig. 8). The result indicates that the dust storm originated from Takalamakan Desert was limited in western China and did not affect the high dust concentrations in eastern China during the SDS period. In addition, the dust storm was also less intensive with the highest dust concentrations of 300 $\mu\text{g}/\text{m}^3$. The weather condition shown in Fig. 4 suggests that the wind speeds nearby the Takalamakan Desert region were weaker compared with the wind speeds in the Gobi Desert region, and the wind direction was toward southeastern Takalamakan Desert. As a result, the dust storm was weaker, and dust storm moved toward the Tibetan Plateau region, which produced important effects

on the Tibetan Plateau glacier due to the strong radiative property of dust particles. However, this later topic is out of the focus of this paper.

The model calculations by including and excluding the PDS are also performed. The net result of the two calculations shows the effect of the PDS on the calculated dust distributions (shown in Fig. 9). The result suggests that on March-19, the PDS had a large effect on dust concentration in the eastern region of Gobi Desert. In addition to the strong dust concentrations originated from Gobi Desert, the PDS enhanced the dust concentrations by about 300 $\mu\text{g}/\text{m}^3$. On March-20, the PDS played important roles in central-eastern China, increasing about 300–400 $\mu\text{g}/\text{m}^3$ dust concentrations in this region. On March-21, the PDS had important effects on the dust concentrations in southern China, and the dust concentrations were enhanced by 200–300 $\mu\text{g}/\text{m}^3$ by the PDS in the downwind regions of Gobi Desert. On March-22, the effect of the PDS was relative small, and the dust concentrations in southern China were underestimated (see Fig. 7).

The above model sensitivity studies suggest that during the SDS event, Gobi Desert play important roles in producing a large amount of dust particles. However, due to the fact that the large dust particles were deposited in the downwind region of the source region, the propagate dust source played important roles in controlling the long range transport of the dust particles in the SDS event.

SUMMARY

Massive dust storms were often occurred in northwestern China and Mongolia deserts during springtime. The massive

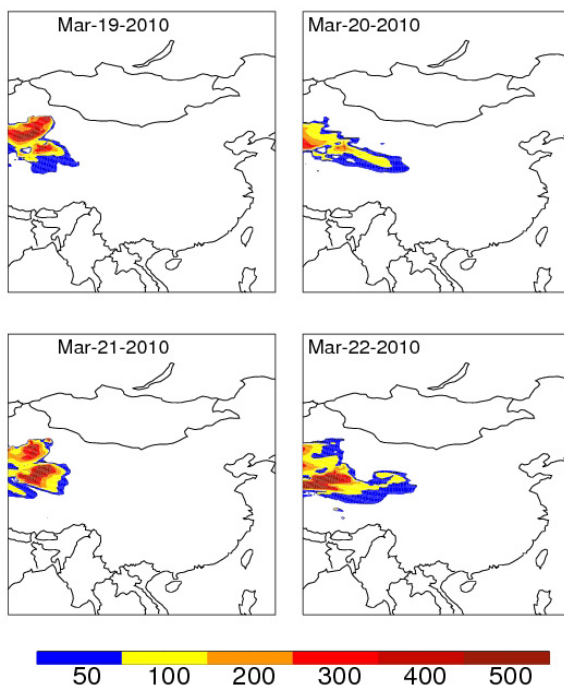


Fig. 8. The calculated dust concentrations ($\mu\text{g}/\text{m}^3$) due to Takalamakan Desert during the SDS period (March-19 to March-22, 2010).

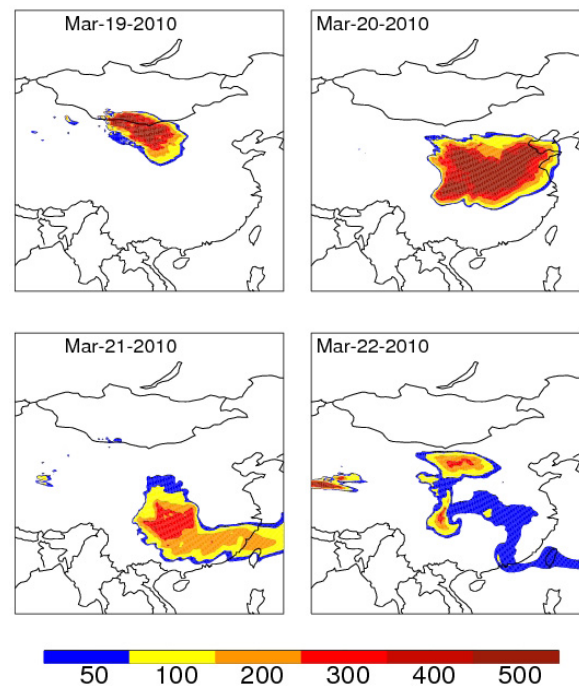


Fig. 9. The calculated dust concentrations ($\mu\text{g}/\text{m}^3$) due to the propagate dust source during the SDS period (March-19 to March-22, 2010).

dust storms have important impacts on environment, human's life, and ecosystem. For example, dust storms produce severe visibility reduction with lowest visibility of less than 200 meters. In this study, a severe dust storm (SDS) event occurred during March-20 to March-22, 2010 in China is analyzed. This SDS event was originated in western China and Mongolia and propagated into eastern/southern China, affecting human's life in a large area. In addition, the dust storm extended in a long period of time (about 4 days). A regional dynamical model (version 3 of Weather Research and Forecasting model – WRF-v3) coupled with a dust model is used in this study. The distribution of nationwide API values was used to trace the dust storm and to compare with the model result. An important objective of this study is to simulate the dust particle distribution and to investigate the processes which play important roles in controlling the severe dust storm (such as its source, transport, and deposition).

The result suggests that in eastern China, the dust pollution is generally produced by 2 large desert regions (i.e., Taklamakan and Gobi Deserts). In this SDS event study, however, the high dust pollution in central-eastern and southeastern China was mainly attributed to Gobi Desert. Another important finding of the study is that large amounts of dust particles were deposited during the transport pathway between the source region and eastern China. The areas where there are heavy surface dust concentrations can be considered as a new dust source region, which produce dust air pollution when surface winds are strong. In this study, we define this process as a propagate dust source (PDS). The model study suggests that the calculated dust concentrations were considerably lower than the measured values in the downwind regions when the PDS process was not included in the model. By including the PDS process, the calculated dust pollution in eastern/southern China is considerably improved. The further detailed analysis shows that the PDS played important roles in controlling the long range transport of dust particles in the SDS event. This study suggests that this regional dynamical/dust model (WRF-Dust) is a useful tool to analyze the important processes of dust storms occurred in China.

ACKNOWLEDGMENTS

The authors would like to thank Steve Peckham and George Grell at NOAA for their help on WRF/Chem model with GOCART dust module. This work is funded by the Tianjin Municipal Science and Technological Administration under Grant no. 10JCYBJC05800, and a special project from Chinese Academy of Sciences (0929011018). The National Center for Atmospheric Research is sponsored by the National Science Foundation.

REFERENCES

- Cao, J.J., Chow, J.C., Watson, J.G., Wu, F., Han, Y.M., Jin, Z.D., Shen, Z.X. and An, Z.S. (2008). Size-differentiated Source Profiles for Fugitive Dust in the Chinese Loess Plateau. *Atmos. Environ.* 42: 2261–2275.
- Chin, M., Ginoux, P., Kinne, S., Torres, O., Holben, B., Duncan, B., Martin, R., Logan, J., Higurashi, A. and Nakajima, T. (2002). Tropospheric Aerosol Optical Thickness from the GOCART Model and Comparisons with Satellite and Sun Photometer Measurements. *J. Atmos. Sci.* 59: 461–483.
- Dayan, U., Heffler, J., Miller, J. and Gutman, G. (1991). Dust Intrusion Events into Mediterranean Basin. *J. Appl. Meteorol.* 30: 1185–1199.
- Duce, R.A., Unni, C.K., Ray, B.J., Prospero, J.M., Merrill, J.T. (1980). Long-range Atmospheric Transport of Soil Dust from Asia to the Tropical North Pacific: Temporal Variability. *Science* 209: 1522–1524.
- Duce, R.A., Liss, C.K., Merrill, J.T., Atlas, E.L., Buat-Menard, P., Hucks, B.B., Miller, J.M., Prospero, J.M., Arimoto, R., Church, T.M., Ellis, W., Galloway, J.N., Hansen, L., Jickells, T.D., Knap, A.H. and Reinhardt, K.H. (1991). The Atmospheric Input of Trace Species to the World Ocean. *Global Biogeochem. Cycles* 5: 193–259.
- Ginoux, P., Chin, M., Tegen, I., Prospero, J., Holben, B., Dubovik, O. and Lin, S.J. (2001). Sources and Distributions of Dust Aerosols Simulated with the GOCART Model. *J. Geophys. Res.* 106: 20255–20273.
- Ginoux, P., Geogdzhayev, I., Holben, B., Stenchikov, G. and Tie, X. (2006). Evaluation of Aerosol Distribution and Optical Depth in GFDL Couple Model. *J. Geophys. Res.* 111: D22210, doi: 10.1029/2005JD006707.
- Grini, A., Myhre, G., Zender, C.S. and Isaksen, I.S.A. (2005). Model Simulations of Dust Sources and Transport in the Global Atmosphere: Effects of Soil Erodibility and Wind Speed Variability. *J. Geophys. Res.* 110: D02205, doi: 10.1029/2004JD005037.
- Gomes, L. and Gillete, D.A. (1993). A Comparison of Characteristics of Aerosol from Dust Storms in Central Asia with Soil-derived Dust from other Regions. *Atmos. Environ.* 27: 2539–2544.
- Gu, Z.L., Wei, W. and Zhao, Y.Z. (2010). An Overview of Surface Conditions in Numerical Simulations of Dust Devils and the Consequent Near-surface Air Flow Fields. *Aerosol Air Qual. Res.* 10: 272–281.
- Hong, S., Noh, Y. and Dudhia, J.A. (2006). A New Vertical Diffusion Package with an Explicit Treatment of Entrainment Processes. *Mon. Weather Rev.* 134: 2318–2341.
- Kim, K.W., Kim, Y.J. and Oh, S.J. (2002). Visibility Impairment during Yellow Sand Periods in the Urban Atmosphere of Kwangju, Korea. *Atmos. Environ.* 35: 5157–5167.
- Lee, B.K., Lee, H.K. and Jun, N.Y. (2009). Analysis of Regional and Temporal Characteristics of PM₁₀ during an Asian Dust Episode in Korea. *Chemosphere* 63: 1106–1115.
- Martcorena, B. and Bergametti, G. (1995). Modeling the Atmospheric Dust Cycle: 1. Design of a Soil-derived Dust Emission Scheme. *J. Geophys. Res.* 100: 16415–16430.
- Mikami, M., Shi, G.Y., Uno, Yabuki, I.S., Iwasaka, Y., Yasui, M., Aoki, T., Tanaka, T.Y., Kurosaki, Y., Masuda,

- K., Uchiyama, A., Matsuki, A., Sakai, T., Takemi, T., M., N. Seino, M. Ishizuka, S. Satake, K. Fujita, Nakawo, Y., Hara, Y., Kai, K., Kanayama, S., Hayashi, M., Du, M., Kanai, Y., Yamada, Y., Zhang, X.Y., Shen, Z., Zhou, H., Abe, O., Nagai, T., Tsutsumi, Y., Chiba, M. and Suzuki, J. (2006). Aeolian Dust Experiment on Climate Impact: An Overview of Japan–China Joint Project ADEC. *Global Planet. Change* 52: 142–172.
- Rost, K.T. (2001). Late Holocene Losses Deposits and Dust Accumulation in the Alpine Meadow Belt of the Wutai Shan, China. *Quat. Int.* 76/77: 85–92.
- Shao, Y. and Dong, C.H. (2006). A Review on East Asian Dust Storm Climate, Modelling and Monitoring. *Global Planet. Change* 52: 1–22.
- Singer, A. (1988). Illite in Aridic Soils, Desert Dusts and Desert Looses. *Sediment. Geol.* 59: 251–259.
- Sokolik, I., Winker, D.M., Bergametti, G., Gillette, D.A., Carmichael, G., Kaufman, Y., Gomes, L., Schuetz, L. and Penner, J.E. (2001). Introduction to Special Section: Outstanding Problems in Quantifying the Radiative Impacts of Mineral Dust. *J. Geophys. Res.* 106: 18015–18028.
- Stone, E.A., Yoon, S.C. and Schauer, J.J. (2011). Chemical Characterization of Fine and Coarse Particles in Gosan, Korea during Springtime Dust Events. *Aerosol Air Qual. Res.* 11: 31–43
- Takayama, Y. and Takashima, T. (1986). Aerosol Optical Thickness Yellow Sand over the Yellow Sea Derived from NOAA Satellite Data. *Atmos. Environ.* 20: 631–638.
- Tie, X. and Cao, J.J. (2009). Aerosol Pollutions in Eastern China; Present and Future Impacts on Environment. *Particuology* 7: 426–431.
- Twomey, S. and Aerosols, A. (1991). Clouds and Radiation, *Atmos. Environ.* 25: 2435–2442.
- Zhang, R.J., Shen, Z.X., Cheng, T.T., Zhang, M.G. and Liu Y.J. (2010). The Elemental Composition of Atmospheric Particles at Beijing during Asian Dust Events in Spring 2004. *Aerosol Air Qual. Res.* 10: 67–75.
- Zhang, Q., Zhao, C., Tie, X., Wei, Q., Li, G. and Li, C. (2006). Characterizations of Aerosols over the Beijing Region: A Case Study of Aircraft Measurements. *Atmos. Environ.* 40: 4513–4527.
- Zhao, J.P., Zhang, F.W., Xu, Y., Chen, J.S., Yin, L.Q., Shang, X.S. and Xu, L.L. (2011). Chemical Characteristics of Particulate Matter during a Heavy Dust Episode in a Coastal City, Xiamen, 2010. *Aerosol Air Qual. Res.* 11: 300–309.
- Zhao, Q., He, K., Rahn, K.A., Ma, Y., Jia, Y., Yang, F., Duan, F., Lei, Y., Chen, G., Cheng, Y., Liu, H. and Wang, S. (2009). Dust Storms Come to Central and Southwestern China, too: Implications from a Major Dust Event in Chongqing. *Atmos. Chem. Phys. Discuss.* 9: 27021–27062.

Received for review, April 26, 2011

Accepted, June 8, 2011